JOURNAL OF GUIDANCE, CONTROL, AND DYNAMICS
Vol. 22, No. 3, May–June 1999

Selective Modal Transducers for Piezolaminated Anisotropic Shells

Scott E. Miller*
Litton Industries, College Park, Maryland 20740
and
Yaakov Oshman† and Haim Abramovich‡
Technion—Israel Institute of Technology, Technion City, 32000 Haifa, Israel

Selective modal transducers (SMTs) are developed for piezolaminated anisotropic zero-Gaussian curvature shell systems that are capable of sensing and exciting any specified set of vibrational modes according to a specified set of modal participation factors. Transduction of selected modes is accomplished through combining the effect of three piezolaminate pairs, whose piezoelectric fields are varied spatially. Each coupled pair contains a single layer located anywhere strictly above the reference plane, which is complemented by a second layer collocated below the reference plane. Piezoelectric constitutive properties associated with each layer in a given couple must be identical, although the constitutive properties of all three couples must be uniquely different. If all SMTs are formed from the same stock material, the stock material must be piezoelectrically biaxial and the skew angles of all couples must be unique. Individual actuator inputs must be proportional to a common control function, or conversely the sensed output must be a weighted sum of the measurements acquired by individual layers. An algorithm is presented that dictates how the piezoelectric field strength of each SMT layer must be varied spatially and that is an explicit function of piezoelectric constants, mode shapes, and designer-chosen modal participation factors. A numerical example is given that both illustrates and validates the SMT design concept.

I. Introduction

WITHIN the past decade several vibration control techniques have been developed for simple beam and plate systems that utilize distributed piezoelectric transducers formed from polyvinylidine fluoride (PVDF).[1,2] PVDF actuators have been designed whose spatially varying piezoelectric field properties were exploited to provide for the simultaneous control of all modes or the selective control of desired modal subsets in cantilevered and simply supported beams.[3] Miller and Hubbard[4,5] developed a reciprocal sensor theory and subsequently incorporated PVDF sensors and actuators into multicomponent systems in which each component itself was a smart structural member. Burke and Hubbard[6] developed a formulation for the control of thin elastic (Kirchhoff–Love) isotropic plates subject to most combinations of free, clamped, or pinned boundary conditions, in which the active elements were spatially varying biaxially polarized piezoelectric transducer layers. Lee generalized the classical laminate theory[7] to include the effect of laminated piezoelectric layers and, thus, to provide a theoretical framework for the distributed transduction of bending, torsion, shearing, shrinking, and stretching in flexible anisotropic plates.[8] Miller et al.[9] subsequently employed Lyapunov's second method to derive a general active vibration suppression control design methodology for anisotropic laminated piezoelectric plates.

The just-mentioned vibration control strategies for both beams and plates share several common limitations. Although all of these methods reduce the vibration control task to a selection of individual piezolaminae field functions, none offers a general method for determining those field functions so as to ensure active vibration suppression. A poor choice in piezofield functions, although guaranteed not to destabilize the structure through the active addition of vibrational energy, may extract little or no vibrational energy from the system. Furthermore, often the designer is concerned with suppressing vibrations in only a certain modal subset. The generalized function approach to choosing spatial field functions,[3,6] although adequate in certain scenarios for guaranteeing some measure of active energy extraction from all modes, generally will not be able to provide a means to selectively target a specific modal subset. Finally, most methodologies mentioned have been exclusive to isotropic systems and are, thus, incompatible for use with orthotropic and anisotropic aeroelastic structures commonly encountered.

For anisotropic plate systems and their derivatives, these limitations have been answered through the development of a selective modal control (SMC) methodology in which the designer optimally utilizes the available piezolaminas so as to most effectively realize any admissible performance objective.[10] Through fully integrating both the structural and control design processes, a broad class of stability robust approaches were defined through the identification of conditions that sufficiently ensure global asymptotic stability without requiring perfect knowledge of design parameters, structural constraints, or modal behavior. Central to the SMC methodology was the development of a selective modal transducer (SMT) theory for anisotropic plates.[11]

In this paper, the SMT theory is extended to include anisotropic zero-Gaussian piezolaminated shells, i.e., curvilinear piezostructures whose geometries are fully deformable onto a plane. SMTs are a class of transducers that are capable of sensing and exciting any specified set of vibrational modes in a selectively weighted fashion. The transduction of selected modal subsets is accomplished through combining the effect of six piezolaminas whose piezoelectric field distributions vary spatially. Design criteria are identified that lead to an algorithm for determining the specific piezoelectric field distributions and scaling factors required of each layer in the composite transducer. The SMC methodology presented in Ref. 10 then becomes fully extensible to this class of shell structures. The paper first presents a concise system description and a Hamiltonian derivation of the equations of motion for anisotropic piezolaminated shells. A general anisotropic SMT shell theory is then developed, and an anisotropic shell SMT numerical example is presented.

Received Oct. 6, 1997; revision received Aug. 7, 1998; accepted for publication Nov. 5, 1998.

*Staff Scientist, Space Systems Operation, Amecom Division, 5115 Calvert Road. Member AIAA.
†Associate Fellow, Department of Aerospace Engineering. Senior Member AIAA.
‡Senior Lecturer, Department of Aerospace Engineering. Senior Member AIAA.

II. System Model Development

A. Geometry

Figure 1 provides a geometric definition of the composite shell structure under consideration. There exist exactly N laminated layers, all of which are considered to be piezoelectrically active: Piezoelectric constants relative to the nonpiezoelectric substructure will be set to zero. The material properties within each lamina are assumed continuous. The electromechanical transduction effect of each lamina may vary spatially. An orthogonal curvilinear coordinate frame is defined by the unit vectors $\hat{\alpha}_1$, $\hat{\alpha}_2$, and $\hat{\alpha}_3$. Piezolaminate sublayers are assumed to be transversely anisotropic, i.e., monoclinic relative to the $\hat{\alpha}_3$ axis. As shown in Fig. 2, the reference surface of the shell is located on the $\alpha_3 = (\alpha_3)_0$ plane. The reference plane itself may be arbitrarily located, although it is typically assigned to the structural midplane. In orthotropic and isotropic structures, however, the reference plane is designated as the neutral plane. Defining the distance in the $\hat{\alpha}_3$ direction between any arbitrary point and the reference plane as z, any arbitrary point $(\alpha_1, \alpha_2, \alpha_3)$ may be equivalently expressed as $[\alpha_1, \alpha_2, (\alpha_3)_0 + z]$. The infinitesimal distance ds between two arbitrary points $(\alpha_1, \alpha_2, \alpha_3)$ and $(\alpha_1 + d\alpha_1, \alpha_2 + d\alpha_2, \alpha_3 + d\alpha_3)$ of a shell element in the curvilinear frame is given as[12]

$$ds^2 = L_1^2(d\alpha_1)^2 + L_2^2(d\alpha_2)^2 + d\alpha_3^2 \tag{1}$$

where the Lamé coefficients L_1 and L_2 are defined as

$$L_1 \triangleq A_1[1 + (z/R_1)], \qquad L_2 \triangleq A_2[1 + (z/R_2)] \tag{2}$$

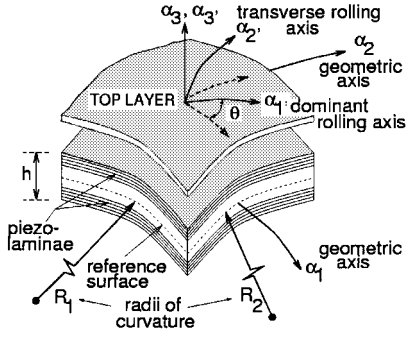

Fig. 1 Geometry of general piezoelectric laminated shell system.

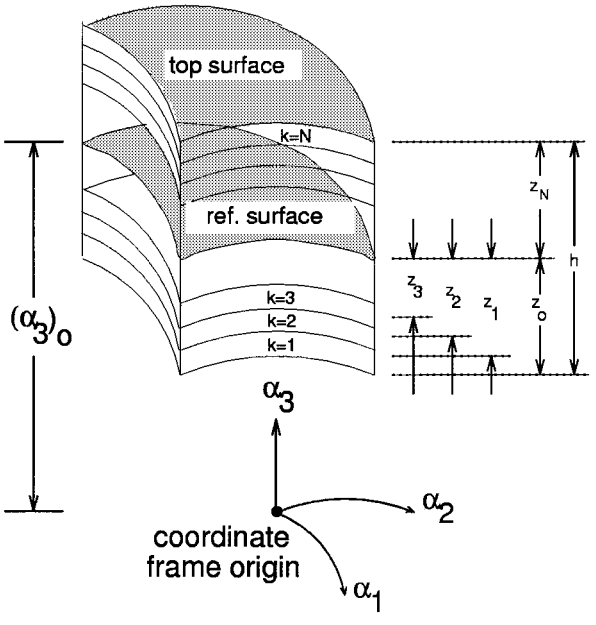

Fig. 2 Lamina coordinate definitions generalized for a coordinate frame whose origin is displaced a distance $(\alpha_3)_0$ from the reference surface.

and A_1 and A_2 are the Lamé parameters.[13] R_1 and R_2 are the radii of curvature corresponding to the $\hat{\alpha}_1$ and $\hat{\alpha}_2$ directions, respectively. Lamé parameters and radii of curvature for several common structural geometries may be found in the literature.[12] The discussion to follow is limited to zero-Gaussian curvature shells, i.e., shell geometries defined such that $1/R_1R_2 = 0$, which include all geometries that are developable onto a plane.

The $\hat{\alpha}_3$ locations of the surfaces of each individual lamina are defined such that the bottom layer of the composite shell is assigned the index $k = 1$, and the indices increase unitarily. The distances from the reference surface to the lower, upper, and middle surfaces of any given lamina are, respectively, defined as z_{k-1}, z_k, and z_k^0. The thickness of any given lamina is defined as h^k. The composite reference surface is displaced at some distance $(\alpha_3)_0$ from the origin of the coordinate frame. The composite thickness is defined as h. The upper and lower surfaces of the composite are located at heights z_N and z_0, respectively.

B. Governing Assumptions

A number of assumptions are made for the derivation of the system equations, in accordance with the classical (nonpiezo) anisotropic laminated cylinder theory of Bert et al.[14]

1) Displacements are small compared to the shell thickness, so that the strain-displacement relations may be assumed to be linear.

2) The Kirchhoff hypothesis is applicable, i.e., line elements normal to the reference surface before deformation remain straight, normal to the deformed reference surface, and unchanged in length after deformation.

3) The ratio of shell thickness to each radius of curvature is small compared with unity so that Love's first-approximation shell theory[15] is applicable $(h/R_1, h/R_2 \ll 1)$.

4) Each lamina is assumed to be in a state of plane stress. Transverse normal and shear strains are neglected.

5) Each individual lamina is assumed to behave macroscopically as an anisotropic, linearly elastic material. Elastic parameters may vary spatially. The mass density and thickness of each layer is uniformly constant.

6) Principal geometric axes of any given layer may be arbitrarily rotated about the $\hat{\alpha}_3$ axis with respect to the principal geometric axes of the shell. If a given layer is piezoelectrically active, its principal geometric axes coincide with its principal piezoelectric rolling and transverse rolling axes.

7) The layers are assumed to be bonded together perfectly such that interlaminar regions are massless and infinitesimally thin.

C. Piezolamina Stress–Strain Behavior

Figure 3 shows the coordinate system of an individual laminate. In Fig. 3 and in the ensuing discussion, a prime superscript will refer to the principal geometric axes of an individual lamina (rolling and transverse rolling axes according to assumption 6). The electrical field distribution of each piezolaminate may be spatially varied by means of varying the surface electrode pattern of each layer. The intensity of electromechanical energy transduction is considered constant through the thickness but may vary spatially as a function of $\alpha_{1'}$ and $\alpha_{2'}$. The elastic moduli of each layer need not be constant throughout the dominant surface of the shell. The influence of the surface electrode layers on the material properties of the lamina is

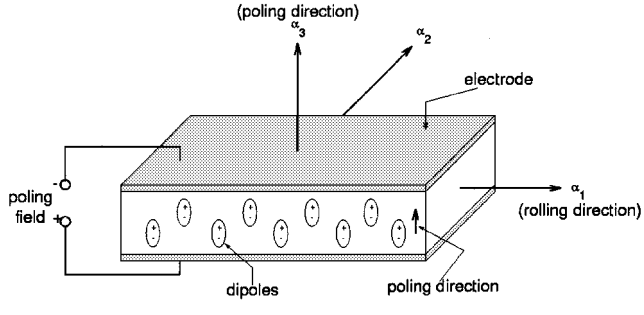

Fig. 3 Geometry of an individual piezoelectric lamina.

neglected. A positive poling direction of each layer is defined as outwardly normal to the geometric midplane of the system.

The stress-strain behavior of each individual lamina is established based on the assumptions listed in Sec. II.B. Adopting Institute of Electrical and Electronics Engineers standard[16] nomenclature, these assumptions lead to the constitutive sublamina strain expression[17]

$$\begin{bmatrix} \epsilon_{1'} \\ \epsilon_{2'} \\ \epsilon_{6'} \end{bmatrix} = \begin{bmatrix} c_{1'1'} & c_{1'2'} & c_{1'6'} \\ c_{1'2'} & c_{2'2'} & c_{2'6'} \\ c_{1'6'} & c_{2'6'} & c_{6'6'} \end{bmatrix} \begin{bmatrix} \sigma_{1'} \\ \sigma_{2'} \\ \sigma_{6'} \end{bmatrix} + \begin{bmatrix} d_{3'1'} \\ d_{3'2'} \\ 0 \end{bmatrix} E_{3'} \tag{3}$$

Referring to each specific lamina by a superscript k, the following definitions are introduced, where the subscript p refers to the principal coordinate frame of the kth lamina:

$$\boldsymbol{\sigma}_p^k, \boldsymbol{\epsilon}_p^k, \boldsymbol{d}_p^k, Q_p^k \triangleq \begin{bmatrix} \sigma_{1'} \\ \sigma_{2'} \\ \sigma_{6'} \end{bmatrix}^k, \begin{bmatrix} \epsilon_{1'} \\ \epsilon_{2'} \\ \epsilon_{6'} \end{bmatrix}^k, \begin{bmatrix} d_{3'1'} \\ d_{3'2'} \\ 0 \end{bmatrix}^k, \begin{bmatrix} Q_{1'1'} & Q_{1'2'} & Q_{1'6'} \\ Q_{1'2'} & Q_{2'2'} & Q_{2'6'} \\ Q_{1'6'} & Q_{2'6'} & Q_{6'6'} \end{bmatrix}^k \tag{4}$$

Using the preceding definitions, Eq. (3) may be inverted and expressed as

$$\boldsymbol{\sigma}_p^k = Q_p^k \boldsymbol{\epsilon}_p^k - Q_p^k \boldsymbol{d}_p^k E_{3'}^k \tag{5}$$

According to Fig. 2, the kth lamina principal axes $\hat{\boldsymbol{\alpha}}_{1'}$ and $\hat{\boldsymbol{\alpha}}_{2'}$ are not coincident with the composite principal geometric axes, but rather are rotated about the $\hat{\boldsymbol{\alpha}}_3$ axis through a skew angle θ^k with respect to the $(\hat{\boldsymbol{\alpha}}_1, \hat{\boldsymbol{\alpha}}_2)$ directions. The following stress and strain transformation laws are then established:

$$\boldsymbol{\sigma}_p^k = T_1 \boldsymbol{\sigma}^k, \qquad \boldsymbol{\epsilon}_p^k = T_2 \boldsymbol{\epsilon}^k \tag{6}$$

where $\boldsymbol{\sigma}^k$ and $\boldsymbol{\epsilon}^k$ are the stress and strain states resolved into the principal composite geometric axes. The transformation matrices are defined as

$$T_1, T_2 \triangleq \begin{bmatrix} m^2 & n^2 & 2mn \\ n^2 & m^2 & -2mn \\ -mn & mn & m^2 - n^2 \end{bmatrix}, \begin{bmatrix} m^2 & n^2 & mn \\ n^2 & m^2 & -mn \\ -2mn & 2mn & m^2 - n^2 \end{bmatrix} \tag{7}$$

where $m \triangleq \cos\theta^k$ and $n \triangleq \sin\theta^k$. The constitutive stress relationship [Eq. (5)] then becomes

$$\boldsymbol{\sigma}^k = Q^k \boldsymbol{\epsilon}^k - \begin{bmatrix} e_{31}^k & e_{32}^k & e_{36}^k \end{bmatrix}^T E_3^k \tag{8}$$

where it is noted that $E_{3'}^k = E_3^k$ and that the material stiffness matrix is defined as $Q^k \triangleq T_1^{-1} Q_p^k T_2$. The piezoelectric constitutive parameters e_{3i}^k are defined according to

$$\begin{bmatrix} e_{31}^k & e_{32}^k & e_{36}^k \end{bmatrix}^T \triangleq T_1^{-1} Q_p^k \boldsymbol{d}_p^k \tag{9}$$

A nontrivial skew angle causes the e_{36} parameter to become nonzero, allowing for the induction and detection of twisting moments and shear forces.

D. Composite Strain Relationships

According to assumption 2 in Sec. II.B, it is assumed that the displacements in the $\hat{\boldsymbol{\alpha}}_1$ and $\hat{\boldsymbol{\alpha}}_2$ directions vary linearly through the shell thickness, whereas the displacements in the $\hat{\boldsymbol{\alpha}}_3$ direction remain independent of α_3:

$$\begin{bmatrix} U(\alpha_1, \alpha_2, \alpha_3) \\ V(\alpha_1, \alpha_2, \alpha_3) \\ W(\alpha_1, \alpha_2, \alpha_3) \end{bmatrix} = \begin{bmatrix} u(\alpha_1, \alpha_2) \\ v(\alpha_1, \alpha_2) \\ w(\alpha_1, \alpha_2) \end{bmatrix} + \alpha_3 \begin{bmatrix} \beta_1(\alpha_1, \alpha_2) \\ \beta_2(\alpha_1, \alpha_2) \\ 0 \end{bmatrix} \tag{10}$$

where U, V, and W describe the displacements of any given point on the structure in the $\hat{\boldsymbol{\alpha}}_1$, $\hat{\boldsymbol{\alpha}}_2$, and $\hat{\boldsymbol{\alpha}}_3$ directions, respectively. The displacements of any given point on the reference surface are described by u, v, and w, whereas β_1 and β_2 represent angles. Neglecting transverse shear deflections (assumption 4), the angles β_1 and β_2 are given by[13]

$$\beta_1 = \frac{u}{R_1} - \frac{1}{A_1}\frac{\partial w}{\partial \alpha_1}, \qquad \beta_2 = \frac{v}{R_2} - \frac{1}{A_2}\frac{\partial w}{\partial \alpha_2} \tag{11}$$

The strain-displacement relationships for a thin shell subject to assumptions 1–5 are given by[13]

$$\epsilon_1 = \frac{1}{A_1}\frac{\partial U}{\partial \alpha_1} + \frac{V}{A_1 A_2}\frac{\partial A_1}{\partial \alpha_2} + \frac{W}{R_1} \tag{12}$$

$$\epsilon_2 = \frac{1}{A_2}\frac{\partial V}{\partial \alpha_2} + \frac{U}{A_1 A_2}\frac{\partial A_2}{\partial \alpha_1} + \frac{W}{R_2} \tag{13}$$

$$\epsilon_6 = \frac{A_2}{A_1}\frac{\partial}{\partial \alpha_1}\left(\frac{V}{A_2}\right) + \frac{A_1}{A_2}\frac{\partial}{\partial \alpha_2}\left(\frac{U}{A_1}\right) \tag{14}$$

Substituting Eqs. (10) and (11) into Eqs. (12–14), separating those terms that are independent of α_3 from those terms linearly dependent on α_3, and recasting into matrix form yields

$$\boldsymbol{\epsilon}^k = [I_3 \quad \alpha_3 I_3] \begin{bmatrix} \boldsymbol{\epsilon}^0 \\ \boldsymbol{\kappa} \end{bmatrix} \tag{15}$$

I_3 is the identity matrix of rank 3, and the vectors $\boldsymbol{\epsilon}^0$ and $\boldsymbol{\kappa}$ are the reference surface membrane and bending (curvature) strains, defined according to

$$\boldsymbol{\epsilon}^0, \boldsymbol{\kappa} \triangleq \begin{bmatrix} \dfrac{1}{A_1}\dfrac{\partial u}{\partial \alpha_1} + \dfrac{u}{A_1 A_2}\dfrac{\partial A_1}{\partial \alpha_2} + \dfrac{w}{R_1} \\ \dfrac{1}{A_2}\dfrac{\partial v}{\partial \alpha_2} + \dfrac{u}{A_1 A_2}\dfrac{\partial A_2}{\partial \alpha_1} + \dfrac{w}{R_2} \\ \dfrac{A_2}{A_1}\dfrac{\partial}{\partial \alpha_1}\left(\dfrac{v}{A_2}\right) + \dfrac{A_1}{A_2}\dfrac{\partial}{\partial \alpha_2}\left(\dfrac{u}{A_1}\right) \end{bmatrix}, \begin{bmatrix} \dfrac{1}{A_1}\dfrac{\partial \beta_1}{\partial \alpha_1} + \dfrac{\beta_2}{A_1 A_2}\dfrac{\partial A_1}{\partial \alpha_2} \\ \dfrac{1}{A_2}\dfrac{\partial \beta_2}{\partial \alpha_2} + \dfrac{\beta_1}{A_1 A_2}\dfrac{\partial A_2}{\partial \alpha_1} \\ \dfrac{A_2}{A_1}\dfrac{\partial}{\partial \alpha_1}\left(\dfrac{\beta_2}{A_2}\right) + \dfrac{A_1}{A_2}\dfrac{\partial}{\partial \alpha_2}\left(\dfrac{\beta_1}{A_1}\right) \end{bmatrix} \tag{16}$$

Note that both $\boldsymbol{\epsilon}^0$ and $\boldsymbol{\kappa}$ are independent of α_3. Because the strains as stated in Eq. (15) vary linearly through the thickness, it has been implicitly recognized that the constitutive strain relationship for each individual lamina is identical. The stresses within each lamina will also vary linearly through the thickness, although the composite stress state will be discontinuous across any interlaminar boundary in which the constitutive material parameters of the adjoining layers are not identical [Eq. (8)]. Introducing the linear and homogeneous differential operator $\mathcal{E}$ defined in the Appendix, Eq. (15) becomes

$$\boldsymbol{\epsilon}^k = [I_3 \quad \alpha_3 I_3][(1/A_1 A_2)\,\mathcal{E}\boldsymbol{x}] \tag{17}$$

where $\boldsymbol{x} = [u \;\; v \;\; w]^T$ is the state vector.

E. Composite Laminate Force and Moment Resultants

The stress state of the composite shell structure may be resolved into a quasistatically equivalent representation of resultant forces and moments acting along the reference surface, whose classical interpretation is found throughout the literature.[7,12,13] Mathematically, the in-plane force resultants ($\boldsymbol{N} \triangleq [N_1 N_2 N_6]^T$) and moment resultants ($\boldsymbol{M} \triangleq [M_1 M_2 M_6]^T$) are defined as

$$\begin{bmatrix} \boldsymbol{N} \\ \boldsymbol{M} \end{bmatrix} = \sum_{k=1}^{N} \int_{z_{k-1}}^{z_k} \begin{bmatrix} I_3 \\ \alpha_3 I_3 \end{bmatrix} \boldsymbol{\sigma}^k \, \mathrm{d}\alpha_3 \tag{18}$$

where

$$\boldsymbol{\sigma} \triangleq \sum_{k=1}^{N} \boldsymbol{\sigma}^k$$

and I_3 is an identity matrix of rank 3. Substituting Eqs. (8) and (17) into Eq. (18) yields

$$\begin{bmatrix} \boldsymbol{N} \\ \boldsymbol{M} \end{bmatrix} = \sum_{k=1}^{k} \int_{z_{k-1}}^{z_k} \left\{ \begin{bmatrix} Q^k & \alpha_3 Q^k \\ \alpha_3 Q^k & \alpha_3^2 Q^k \end{bmatrix} \frac{1}{A_1 A_2} \mathcal{E}\boldsymbol{x} - \begin{bmatrix} I_3 \\ \alpha_3 I_3 \end{bmatrix} \begin{bmatrix} e_{31}^k & e_{32}^k & e_{36}^k \end{bmatrix}^T E_3^k \right\} \mathrm{d}\alpha_3 \tag{19}$$

Defining the kth piezolamina driving voltage as $V^k(t) = h^k E_3^k(t)$ and integrating Eq. (19) yields

$$\begin{bmatrix} \boldsymbol{N} \\ \boldsymbol{M} \end{bmatrix} = \begin{bmatrix} A & B \\ B & D \end{bmatrix} \frac{1}{A_1 A_2} \mathcal{E}\boldsymbol{x} - \sum_{k=1}^{N} \boldsymbol{e}^k V^k \tag{20}$$

where A, B, D represent equivalent composite material parameters defined by

$$(A, B, D) \triangleq \sum_{k=1}^{N} \int_{z_{k-1}}^{z_k} \left(1, \alpha_3, \alpha_3^2\right) Q^k \, \mathrm{d}\alpha_3 \tag{21}$$

and the vector $\boldsymbol{e}^k$ is defined as

$$\boldsymbol{e}^k \triangleq \begin{bmatrix} e_{31}^k & e_{32}^k & e_{36}^k & z_k^0 e_{31}^k & z_k^0 e_{32}^k & z_k^0 e_{36}^k \end{bmatrix}^T \tag{22}$$

[Note there is an ambiguity regarding the sign definition of $V^k(t)$ that is addressed specifically in Ref. 17.]

F. Piezoelectric Field Distribution Functions

The spatially varying behavior of the electromechanical transduction effect, typically accomplished through doping or repoling processes,[18] is introduced through consideration of a dimensionless, spatially varying piezoelectric field distribution function (PFF), $\Lambda^k(\alpha_1, \alpha_2)$. The field function is defined such that the piezoelectric field vector $\boldsymbol{e}^k$ is equivalently expressed in the form

$$\begin{aligned} \boldsymbol{e}^k &= \left[\left(e_{31}^k\right)_0 \ \left(e_{32}^k\right)_0 \ \left(e_{36}^k\right)_0 \ z_k^0 \left(e_{31}^k\right)_0 \ z_k^0 \left(e_{32}^k\right)_0 \ z_k^0 \left(e_{36}^k\right)_0 \right]^T \Lambda^k \\ &= \boldsymbol{e}_0^k \Lambda^k \end{aligned} \tag{23}$$

The piezoelectric constants $(e_{31}^k)_0$, $(e_{32}^k)_0$, and $(e_{36}^k)_0$ are arbitrarily defined as the values of e_{31}^k, e_{32}^k, and e_{36}^k at the point of maximum electromechanical transduction so that Λ^k is normalized, i.e., the maximum value of Λ^k is unity. For convenience in the ensuing analyses the vector $\boldsymbol{e}_*^k$ is also defined such that

$$\boldsymbol{e}_*^k \triangleq \begin{bmatrix} \left(e_{31}^k\right)_0 & \left(e_{32}^k\right)_0 & \left(e_{36}^k\right)_0 \end{bmatrix} \tag{24}$$

Substitution of Eq. (23) into Eq. (20) then yields

$$\begin{bmatrix} \boldsymbol{N} \\ \boldsymbol{M} \end{bmatrix} = \frac{1}{A_1 A_2} \begin{bmatrix} A & B \\ B & D \end{bmatrix} \mathcal{E}\boldsymbol{x} - \sum_{k=1}^{N} \boldsymbol{e}_0^k \Lambda^k V^k \tag{25}$$

G. Equations of Motion

From Hamilton's principle it is known that a geometrically admissible motion of a conservative system between prescribed configurations at arbitrary times t_0 and t_1 satisfies the geometric dynamic force requirements if and only if

$$\delta \int_{t_0}^{t_1} [\mathcal{T} - \mathcal{U}] \, \mathrm{d}t = 0 \tag{26}$$

where the symbol δ indicates geometric variation. $\mathcal{T}$ and $\mathcal{U}$ are defined as the system kinetic and potential energy states, respectively. The potential energy state includes both mechanical energy and electrical enthalpy terms and is defined as[16]

$$\mathcal{U} \triangleq \sum_{k=1}^{N} \left\{ \int\int\int_{\mathcal{V}} \left[\frac{1}{2} (\boldsymbol{\epsilon}^k)^T Q^k \boldsymbol{\epsilon}^k - \begin{bmatrix} e_{31}^k & e_{32}^k & e_{36}^k \end{bmatrix} \boldsymbol{\epsilon}^k E_3^k - \frac{1}{2} \varepsilon_{33}^k \left(E_3^k\right)^2 \right] \mathrm{d}\mathcal{V} + q^k V^k \right\} \tag{27}$$

where $\mathrm{d}\mathcal{V} = A_1 A_2 \, \mathrm{d}\alpha_1 \, \mathrm{d}\alpha_2 \, \mathrm{d}\alpha_3$ is a differential volumetric element, $\mathcal{V}$ is the total volume of the kth layer, and ε_{33}^k is the electrical permittivity of the kth layer. The final term on the right-hand side (RHS) of the expression (27) represents electrical work due to a static charge on the kth layer subjected to an applied voltage field. Substituting Eq. (17) into expression (27) and integrating with respect to α_3 from z_{k-1} to z_k yields

$$\mathcal{U} = \sum_{k=1}^{N} \left\{ \int\int_{A} \left[\frac{1}{2} \left(\frac{1}{A_1 A_2} \mathcal{E}\boldsymbol{x} \right)^T \begin{bmatrix} A & B \\ B & D \end{bmatrix} \left(\frac{1}{A_1 A_2} \mathcal{E}\boldsymbol{x} \right) - \left(\frac{1}{A_1 A_2} \mathcal{E}\boldsymbol{x} \right)^T \boldsymbol{e}_0^k \Lambda^k V^k - \frac{1}{2} \left(\frac{\varepsilon_0^k}{h^k} \Lambda^k \right) (V^k)^2 \right] \mathrm{d}A + q^k V^k \right\} \tag{28}$$

where the field distribution function Λ^k has been introduced via Eqs. (23). Maximum permittivity in the kth lamina, ε_0^k, has been defined such that $\varepsilon_{33}^k = \Lambda^k \varepsilon_0^k$.

The total first variation in $\mathcal{U}$ may be expressed as

$$\delta\mathcal{U} = (\mathcal{U})_{\boldsymbol{x}}^T \delta\boldsymbol{x} + \sum_{k=1}^{N} (\mathcal{U})_{V^k} \delta V^k \tag{29}$$

where $(\mathcal{U})_{\boldsymbol{x}}$ and $(\mathcal{U})_{V^k}$ are the first partial derivatives of $\mathcal{U}$ with respect to both the displacement field vector and the applied voltage field, respectively. Carrying out the variation with respect to V^k,

$$\sum_{k=1}^{N} (\mathcal{U})_{V^k} \delta V^k = \sum_{k=1}^{N} \left[q^k - \int\int_{A} \frac{1}{A_1 A_2} (\mathcal{E}\boldsymbol{x})^T \boldsymbol{e}_0^k \Lambda^k \, \mathrm{d}A - C_p^k V^k \right] \delta V^k \tag{30}$$

where the capacitance C_p^k of the kth layer is defined as

$$C_p^k \triangleq \int\int_{A} \frac{\varepsilon_0^k}{h^k} \Lambda^k \, \mathrm{d}A \tag{31}$$

Recalling Eq. (25) and carrying out the variation with respect to $\boldsymbol{x}$,

$$(\mathcal{U})_{\boldsymbol{x}}^T \delta\boldsymbol{x} = \int\int_{A} \left[\frac{1}{A_1 A_2} \mathcal{E}(\delta\boldsymbol{x}) \right]^T \begin{bmatrix} \boldsymbol{N} \\ \boldsymbol{M} \end{bmatrix} \mathrm{d}A \tag{32}$$

Integrating Eq. (32) by parts,

$$(\mathcal{U})_{\boldsymbol{x}}^T \delta\boldsymbol{x} = \int\int_{A} \delta\boldsymbol{x}^T \left\{ \frac{1}{A_1 A_2} \mathcal{D}^T \begin{bmatrix} \boldsymbol{N} \\ \boldsymbol{M} \end{bmatrix} \right\} \mathrm{d}A + I_1 + I_2 \tag{33}$$

where

$$I_1 = \int_{\alpha_2^*} A_2[(N_1)\delta u + (N_6)\delta v + (Q_4)\delta w + (M_1)(\delta\beta_1) + (M_6)(\delta\beta_2)]_{\alpha_1^*}\,\mathrm{d}\alpha_2 \tag{34}$$

$$I_2 = \int_{\alpha_1^*} A_1[(N_6)\delta u + (N_2)\delta v + (Q_5)\delta w + (M_6)(\delta\beta_1) + (M_2)(\delta\beta_2)]_{\alpha_2^*}\,\mathrm{d}\alpha_1 \tag{35}$$

and $\mathcal{D}$, Q_4, and Q_5 are defined in the Appendix. The symbols α_1^* and α_2^* refer to boundary limits along α_1 and α_2, respectively.

The kinetic energy is defined as

$$\mathcal{T} \triangleq \frac{1}{2}\int\int_A \rho h \boldsymbol{x}_t^T \boldsymbol{x}_t\,\mathrm{d}A$$

so that on integration by parts its variation is given as

$$\delta\mathcal{T} = \int\int_A \delta\boldsymbol{x}\cdot(-\rho h\boldsymbol{x}_{tt})\,\mathrm{d}A \tag{36}$$

Substituting Eqs. (29), (30), (33), and (36) into Eq. (26) then yields

$$\int_{t_0}^{t_1}\mathrm{d}t\left\{\delta\boldsymbol{x}^T\left[\int\int_A\left(\rho h\boldsymbol{x}_{tt} + \frac{1}{A_1A_2}\mathcal{D}^T\begin{bmatrix}\boldsymbol{N}\\ \boldsymbol{M}\end{bmatrix}\right)\mathrm{d}A\right] + \sum_{k=1}^{N}\delta V^k\left[q^k - \int\int_A\frac{1}{A_1A_2}(\mathcal{E}\boldsymbol{x})^T\boldsymbol{e}_0^k\Lambda^k\,\mathrm{d}A - C_p^kV^k\right]\right\} + I_1 + I_2 = 0 \tag{37}$$

Hence, when the system is perturbed by an arbitrary admissible variation, the preceding equality holds only if

$$\rho h\boldsymbol{x}_{tt} + \frac{1}{A_1A_2}\mathcal{D}^T\begin{bmatrix}\boldsymbol{N}\\ \boldsymbol{M}\end{bmatrix} = 0 \tag{38}$$

and

$$q^k(t) = \int\int_A\frac{1}{A_1A_2}(\mathcal{E}\boldsymbol{x})^T\boldsymbol{e}_0^k\Lambda^k\,\mathrm{d}A + C_p^kV^k \tag{39}$$

Substitution of Eq. (25) into Eq. (38) then yields

$$\boldsymbol{x}_{tt} + \mathcal{K}\boldsymbol{x} = \frac{1}{\rho hA_1A_2}\mathcal{D}^T\left(\sum_{k=1}^{N}\boldsymbol{e}_0^k\Lambda^kV^k\right) \tag{40}$$

where the (mass-normalized) stiffness operator $\mathcal{K}$ is defined as

$$\mathcal{K} \triangleq \frac{1}{\rho hA_1A_2}\mathcal{D}^T\frac{1}{A_1A_2}\begin{bmatrix}A & B\\ B & D\end{bmatrix}\mathcal{E} \tag{41}$$

Damping may be introduced in the model through a damping operator that is proportional to both the (mass-density-normalized) stiffness operator $\mathcal{K}$ and the identity operator $\mathcal{I}$ by positive factors b_0 and c_0 (Ref. 19):

$$\mathcal{C} = b_0\mathcal{I} + c_0\mathcal{K} \tag{42}$$

Consequently, Eq. (40) becomes

$$\boldsymbol{x}_{tt} + \mathcal{C}\boldsymbol{x}_t + \mathcal{K}\boldsymbol{x} = \frac{1}{\rho hA_1A_2}\mathcal{D}^T\left(\sum_{k=1}^{N}\boldsymbol{e}_0^k\Lambda^kV^k\right) \tag{43}$$

Equations (39) and (43) are the equations of motion for a composite piezoelectric thin shell. Mechanical boundary conditions, given in Table 1, are derived via the boundary integrals (I_1, I_2). The mechanical boundary conditions are stated in Poisson's form for convenience but are readily reducible to four conditions per edge (Kirchhoff form).[12] Equation (39) is the (definite) integral form of the electrostatic charge displacement equation for this class of materials and was derived through the implicit assumption that the standard electrical continuity conditions[16] are applicable at interlaminar and air-dielectric interfaces.

Table 1 Boundary conditions for a general thin shell (Poisson form)

$\alpha_1 = \alpha_1^*$	$\alpha_2 = \alpha_2^*$
N_1 or u	N_2 or v
N_6 or v	N_6 or u
Q_1 or w	Q_2 or w
M_1 or β_1	M_2 or β_2
M_6 or β_2	M_6 or β_1

Equation (39) may be rendered into more useful and advantageous forms by recalling that the measured current is by definition the time derivative of the developed charge, and the voltage measured across the electrode surfaces is found by dividing the developed charge by the film capacitance. In practice an output measurement that is directly related to mechanically induced strain is desired. Thus, the most useful sensor current or voltage relationships are found by manipulating Eq. (39) such that

$$i_s^k(t) = i_m^k(t) - C_p^k\frac{\mathrm{d}V^k}{\mathrm{d}t} = \int\int_A\frac{1}{A_1A_2}(\mathcal{E}\boldsymbol{x}_t)^T\boldsymbol{e}_0^k\Lambda^k\,\mathrm{d}A \tag{44}$$

$$V_s^k(t) = V_m^k(t) - V^k(t) = \frac{1}{C_p^k}\int\int_A\frac{1}{A_1A_2}(\mathcal{E}\boldsymbol{x})^T\boldsymbol{e}_0^k\Lambda^k\,\mathrm{d}A \tag{45}$$

where $i_m^k(t)$ and $V_m^k(t)$ are the kth lamina current and voltage direct measurements. The consequence of Eqs. (44) and (45) is that the same piezoelectric layer may be used simultaneously both as a sensor and as an actuator through the use of differential circuitry and electronics.[20] This capability is exploited in the SMT development to follow.

H. Stiffness Operator Domain

The domain of definition for the operator $\mathcal{K}$ (and, thus, $\mathcal{C}$) is now explicitly defined. Let the Hilbert space of all real-valued piecewise continuous functions $\boldsymbol{g}(\alpha_1,\alpha_2)$, $\boldsymbol{h}(\alpha_1,\alpha_2) \in A$ whose inner product and norm are, respectively, defined as

$$\langle\boldsymbol{g},\boldsymbol{h}\rangle = \int_A\boldsymbol{g}^T\boldsymbol{h}\,\mathrm{d}A, \qquad \|\boldsymbol{g}\| = \langle\boldsymbol{g},\boldsymbol{g}\rangle^{\frac{1}{2}}$$

be denoted as $H(A)$. Designating the order of $\mathcal{K}$ as l, let any admissible set of boundary conditions given in Table 1 be described in terms of linear spatial differential operators $\mathcal{B}_i$ of maximum order $l-1$ such that

$$\mathcal{B}_i\boldsymbol{x} = 0 \quad \text{on} \quad \Gamma, \qquad i = 1,\ldots,l \tag{46}$$

Let S be the set of all functions $\boldsymbol{g}$ for which $\mathcal{B}_i\boldsymbol{g} = 0$ on Γ and such that $\boldsymbol{g}$ and all of its l derivatives are in $H(A)$. In the ensuing development, the admissible set of boundary conditions to be considered is such that $\mathcal{K}$ is rendered regular on S and has an inverse defined by a Green's function. Note that any set of boundary conditions that does not permit rigid-body motions automatically satisfies this criterion. A procedure for explicitly determining the Green's function inverse is given in Ref. 13.

III. SMT Theory

A. General Design Methodology

In this section an SMT theory is presented that allows for the selective excitation and detection of each and every mode of an anisotropic piezolaminated thin shell. Inman[21] restated the result of Caughey and O'Kelly[22] as follows.

Theorem 1. Let $\boldsymbol{x}_{tt} + \mathcal{C}\boldsymbol{x}_t + \mathcal{K}\boldsymbol{x} = \boldsymbol{f}(\alpha_1,\alpha_2,t)$ describe the equations of motion of a general system excited by a distributed force $\boldsymbol{f}$. Then, if $\mathcal{C}$ and $\mathcal{K}$ commute and are self-adjoint on S, and if each operator has an inverse defined by a Green's function, the

solution to the governing equation may be written as the uniformly convergent series

$$\boldsymbol{x}(\alpha_1, \alpha_2, t) = \sum_{j=1}^{\infty} \boldsymbol{\phi}_j(\alpha_1, \alpha_2) q_j(t) \tag{47}$$

where $\{\boldsymbol{\phi}_j(\alpha_1, \alpha_2)\}_{j=1}^{\infty}$ is the set of orthonormal eigenfunctions of $\mathcal{K}$ that are identical to the eigenfunctions of $\mathcal{C}$.

The operators $\mathcal{C}$ and $\mathcal{K}$ are proven in Ref. 23 to be self-adjoint on S, and moreover, it is trivial to ascertain from Eq. (42) that both operators commute, i.e., $\mathcal{C}\mathcal{K} = \mathcal{K}\mathcal{C}$. It has also been presupposed that the boundary conditions are such that $\mathcal{K}$ (and, thus, $\mathcal{C}$) has a Green's function inverse. The following lemma may therefore be stated based on Theorem 1.

Lemma 1. Define $\bar{\phi}$ as

$$\bar{\phi} \triangleq \sum_{j=1}^{\infty} \alpha_j \phi_j, \qquad \alpha_j \in \Re^1 \tag{48}$$

Then, if an anisotropic thin shell of area A is excited by a distributed force of the form $\boldsymbol{f} = V_a(t)\mathcal{K}\bar{\phi}$, the equations of motion of the system are reduced to the form

$$\ddot{q}_m + (b_0 + c_0\lambda)\dot{q}_m + \lambda_m q_m = \alpha_m \lambda_m V_a(t) \tag{49}$$

for all integers $m > 0$.

Remark. The parameters α_j are henceforth referred to as modal participation factors (MPFs).

Proof. The set of eigenfunctions $\{\phi_j\}_{j=1}^{\infty}$ is complete and spans $H(A)$, $\bar{\phi} \in S$; moreover, all conditions in Theorem 1 are satisfied. Replacing the RHS of Eq. (43) with $V_a(t)\mathcal{K}\bar{\phi}$ and applying Eq. (47),

$$\sum_{j=1}^{\infty} [\phi_j \ddot{q}_j + (b_0 + c_0\mathcal{K})\phi_j \dot{q}_j + \mathcal{K}\phi_j q_j] = V_a(t) \sum_{j=1}^{\infty} \alpha_j \mathcal{K}\phi_j \tag{50}$$

The modal orthonormality condition for anisotropic thin piezolaminated shells is given as[23]

$$\langle \phi_i, \phi_j \rangle = \delta_{ij} \tag{51}$$

where δ_{ij} is the Kronecker delta function. Because $\mathcal{K}\phi_j = \lambda_j \phi_j$, where λ_j is the eigenvalue corresponding to the jth eigenfunction, a related condition is immediately established from Eq. (51):

$$\langle \phi_i, \mathcal{K}\phi_j \rangle = \lambda_j \delta_{ij} \tag{52}$$

Taking the inner product of the mth eigenfunction ϕ_m with each side of Eq. (50) and applying Eqs. (51) and (52) then returns Eq. (49) for all integers $m > 0$. □

Consider the following set of design constraints.

Condition 1. Exactly n transducer layers are located strictly above the reference surface, and exactly n transducers are located strictly below the reference surface ($N = 2n$).

Condition 2. There are at least six piezoelectrically active layers ($2n \geq 6$).

Condition 3. For each layer above the reference surface there exists a layer below the reference surface such that $\{z^k = -z^{k+n}\}_{k=1}^{n}$.

Condition 4. Layers located at heights z^k and z^{k+n} both are associated with the identical piezoproperty vector $\boldsymbol{e}_*^k$.

Condition 5. The piezoproperty vectors $\{\boldsymbol{e}_*^k\}_{k=1}^{n}$ associated with at least three layers above and likewise below the reference surface are different. When the same piezostock material is used throughout, $e_{31}^0(\theta^k = 0) \neq e_{32}^0(\theta^k = 0)$ deg and the skew angles of at least six laminas above (and likewise below) the surface must be different in the range $-90 \leq \theta^k < 90$ deg.

The following lemma is now introduced.

Lemma 2. Let $R \in \Re^{6,6}$ be the matrix defined as

$$R \triangleq \sum_{k=1}^{N} \boldsymbol{e}_0^k \left(\boldsymbol{e}_0^k\right)^T \tag{53}$$

Then, if conditions 1–5 hold, R is invertible. Furthermore, R can be written as

$$R = 2\sum_{k=1}^{n} \begin{bmatrix} \boldsymbol{e}_*^k \left(\boldsymbol{e}_*^k\right)^T & \boldsymbol{0} \\ \boldsymbol{0} & (z^k)^2 \boldsymbol{e}_*^k \left(\boldsymbol{e}_*^k\right)^T \end{bmatrix} \tag{54}$$

Proof. Substituting Eq. (23) into Eq. (53) yields

$$R = \sum_{k=1}^{N} \begin{bmatrix} \boldsymbol{e}_*^k \left(\boldsymbol{e}_*^k\right)^T & z^k \boldsymbol{e}_*^k \left(\boldsymbol{e}_*^k\right)^T \\ z^k \boldsymbol{e}_*^k \left(\boldsymbol{e}_*^k\right)^T & (z^k)^2 \boldsymbol{e}_*^k \left(\boldsymbol{e}_*^k\right)^T \end{bmatrix} \tag{55}$$

Satisfying conditions 1, 3, and 4 then transforms R into the form

$$R = 2\begin{bmatrix} \sum_{k=1}^{n} \boldsymbol{e}_*^k \left(\boldsymbol{e}_*^k\right)^T & \boldsymbol{0} \\ \boldsymbol{0} & \sum_{k=1}^{n} \left(z^k \boldsymbol{e}_*^k\right)\left(z^k \boldsymbol{e}_*^k\right)^T \end{bmatrix} \tag{56}$$

which is equivalent to Eq. (54). Conditions 2 and 5 are seen to be necessary for the invertibility of the submatrices located on the diagonal of the rightmost term, based on the following lemma.[23]

Lemma 3. Given a set of column vectors $\{\boldsymbol{r}_k : \boldsymbol{r}_k \in \Re^m\}$, the matrix

$$R_0 \triangleq \sum_{k=1}^{n} \boldsymbol{r}_k \boldsymbol{r}_k^T$$

is invertible if and only if there exist at least m linearly independent vectors in the set $\{\boldsymbol{r}_k\}_{k=1}^{n}$. The consequence of Lemma 3 is that the submatrices on the diagonal of the rightmost expression in Eq. (56) are invertible only if $n \geq 3$ and at least three elements of each vector subset $\{\boldsymbol{e}_*^k\}_{k=1}^{n}$ and $\{z^k \boldsymbol{e}_*^k\}_{k=1}^{n}$ are unique. Condition 1 ensures that all z^k are nonzero, and the physical geometry ensures that all z^k are different. Condition 2 and the first part of condition 5 then cause the elements of each vector subset to be independent. The latter part of condition 5 pertains to the event in which the same sample of piezoelectric material is chosen to construct every active layer in the structure. In such a case it is necessary that $e_{31}^0(\theta^k = 0) \neq e_{32}^0(\theta^k = 0)$ deg and that the skew angles of laminas above (and likewise below) the surface must be different in the range[23] $-90 \leq \theta^k < 90$ deg. Obeying this constraint causes the piezoelectric field properties of each of the n piezolaminas above (and likewise below) the reference surface to be uniquely different with respect to the principal geometric directions. □

The general SMT theorem is now stated.

Theorem 2. Consider an anisotropic (Kirchhoff–Love) thin shell containing N piezolaminas whose equations of motion are given by Eq. (43). Assume that each lamina is to function as a self-sensing actuator such that the sensed measurement of the kth layer is given by Eq. (44). Let the measured state $i_s(t)$ be formed from the weighted sum of the sensed currents of each individual lamina such that

$$i_s(t) = \sum_{k=1}^{N} g_0^k i_s^k(t)$$

Let the time-bound control input $V^k(t)$ of each piezolamina be proportional to an identical time-dependent control function $V_a(t)$ such that $V^k(t) = g_0^k V_a(t)$. Assume that conditions 1–5 are satisfied. If the PFFs of each active layer are given by

$$\Lambda^k = \frac{1}{g_0^k} \left(\boldsymbol{e}_0^k\right)^T R^{-1} \frac{1}{A_1 A_2} \begin{bmatrix} A & B \\ B & D \end{bmatrix} \mathcal{E}\bar{\phi} \tag{57}$$

where the weighted modal sum $\bar{\phi}$ is defined in Eq. (48), the invertible constant matrix R is defined in Eq. (54), and the scaling factor g_0 is defined as

$$g_0^k = \max_{(\alpha_1, \alpha_2) \in A} \left| \left(\boldsymbol{e}_0^k\right)^T R^{-1} \frac{1}{A_1 A_2} \begin{bmatrix} A & B \\ B & D \end{bmatrix} \mathcal{E}\bar{\phi} \right| \tag{58}$$

Then the measured state is reduced to the form

$$i_s(t) = \rho h \sum_{j=1}^{\infty} \alpha_j \lambda_j \dot{q}_j(t) \tag{59}$$

and the equations of motion of the shell are reduced to the form

$$\ddot{q}_j + (b_0 + c_0\lambda)\dot{q}_j + \lambda_j q_j = \alpha_j \lambda_j V_a(t) \tag{60}$$

for all integers $j > 0$, where α_j, λ_j, and $\dot{q}_j$ are, respectively, the modal participation factor, eigenvalue, and generalized modal velocity associated with the jth eigenfunction.

Proof. Substituting $V^k(t) = g_0^k V_a(t)$ and Eq. (57) into the RHS of Eq. (43) and applying Lemma 2 yields [recall Eq. (41)]

$$\boldsymbol{x}_{tt} + \mathcal{C}\boldsymbol{x}_t + \mathcal{K}\boldsymbol{x} = V_a(t)\,\mathcal{K}\bar{\phi} \tag{61}$$

Equation (61) is in the form supposed by Lemma 1, and thus the equations of motion are reduced to Eq. (49), which is synonymous with Eq. (60).

Recalling that $dA = A_1 A_2\, d\alpha_1\, d\alpha_2$, the stipulation that

$$i_s(t) = \sum_{k=1}^{N} g_0^k i_s^k(t)$$

transforms Eq. (44) into the form

$$i_s(t) = \int\int_A (\mathcal{E}\boldsymbol{x}_t)^T \left(\sum_{k=1}^{N} g_0^k \boldsymbol{e}_0^k \Lambda^k \right) d\alpha_1\, d\alpha_2 \tag{62}$$

Substituting Eq. (57) into Eq. (62) and applying Lemma 2 yields

$$i_s(t) = \int\int_A \frac{1}{A_1 A_2} (\mathcal{E}\boldsymbol{x}_t)^T \begin{bmatrix} A & B \\ B & D \end{bmatrix} (\mathcal{E}\bar{\phi})\, d\alpha_1\, d\alpha_2 \tag{63}$$

Substituting Eqs. (47) and (48) into Eq. (63),

$$i_s(t) = \sum_{i=1}^{\infty}\sum_{j=1}^{\infty} \alpha_j \dot{q}_i \int\int_A \frac{1}{A_1 A_2} (\mathcal{E}\phi_i)^T \begin{bmatrix} A & B \\ B & D \end{bmatrix} (\mathcal{E}\phi_j)\, d\alpha_1\, d\alpha_2 \tag{64}$$

Integrating the RHS of Eq. (64) by parts and applying the boundary conditions found in Table 1 yields[23]

$$i_s(t) = \rho h \sum_{i=1}^{\infty}\sum_{j=1}^{\infty} \alpha_j \dot{q}_i [\langle \phi_i,\, \mathcal{K}\phi_j \rangle] \tag{65}$$

which is reduced to Eq. (59) via Eq. (52). □

Equations (59) and (60) imply that one may selectively sense and excite any given mode or subset of modes in the structure, which leads naturally to the following corollary.

Corollary 1. When all suppositions of Theorem 2 are satisfied, the system is completely controllable and observable.

B. Discussion

Having established Theorem 2, an anisotropic piezolaminated SMT theory has been defined. By obeying those conditions stipulated in the theorem, a self-sensing actuator may be developed whose measurement and excitation are selectively weighted in the system modal space. The theory is readily extended to dedicated modal sensors or modal actuators through simplifications that are assumed to be obvious. The general theory may be straightforwardly reduced to directly address orthotropic and isotropic shell structures.[23] Isotropic systems can be shown to require only a single piezolayer as a sufficient condition for complete controllability and observablity. Orthotropic systems can be similarly shown to require only three layers.

An SMT design methodology is thus presented: a modal subset is selected, subset mode shapes are identified, and MPFs are chosen; the stipulated design conditions are then obeyed and Eq. (57) is applied. Although practical limitations, e.g., piezoelectric sublayer inhomogeneity, may impede perfect implementation of the design methodology, experimental results on a multilayered orthotropic piezoplate show that often the methodology can be applied without significant degradation.[24] Nonetheless, a companion nonselective modal transducer theory has been developed[11,23] based on Theorem 2, which allows the modal character of a given piezotransducer to be determined directly. Greater fidelity in the design process could be accomplished through an iterative design process that incorporates both theories.

IV. Numerical Example: Cylindrical Panel

The SMT design concept is both illustrated and validated through a numerical example involving a cantilevered cylindrical panel whose geometry is given in Fig. 4. The panel itself is a cylindrical semisection, which spans 60 deg of a cylinder with a fixed radius R, such that the (α_2-dimension) width is 0.4 m. The section length is 0.6 m. Three mechanically isotropic and piezoelectrically biaxial PVDF layers are bonded to each surface of a double-layered graphite–epoxy (G–epoxy) composite substrate, and the layers are sequentially numbered from top (layer 1) to bottom (layer 8). Relevant material properties are given in Tables 2 and 3.

A discrete model of the passive system was developed based on a 169-node finite element representation of the plate using the

Table 2 Material properties for example structure

Property	PVDF	G–epoxy
E_{11}, Pa	2.00×10^9	14.5×10^9
E_{22}, Pa	2.00×10^9	9.60×10^9
G_{12}, Pa	1.42×10^9	4.10×10^9
ν_{12}	0.3	0.3
ρ, kg/m^3	1780	1551
$(e_{31}^0)_{\theta=0\ \mathrm{deg}}$, C/m^2	60×10^3	——
$(e_{32}^0)_{\theta=0\ \mathrm{deg}}$, C/m^2	20×10^3	——

Table 3 Sublaminae skew angles and thicknesses

	PVDF (top)			G–epoxy (middle)		PVDF (bottom)		
Layer	1	2	3	4	5	6	7	8
Skew angle, deg	60	0	−60	45	−45	−60	0	60
Thickness, μm	28	28	28	140	140	28	28	28

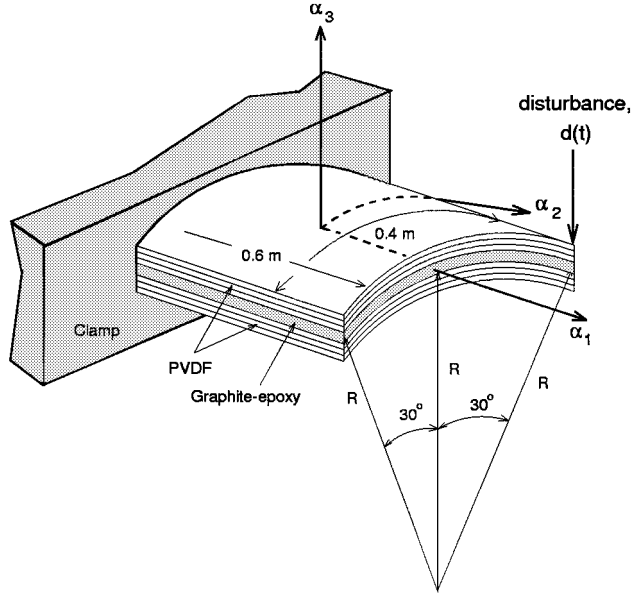

Fig. 4 Cylindrical panel example problem geometry.

Table 4 Damping coefficients and natural frequencies

Mode	ζ_m	ω_m, rad/s
1	0.00748	29.93
2	0.01473	58.91
3	0.03583	143.3
4	0.03594	145.8
5	0.03898	155.9
6	0.04395	175.8
7	0.06420	256.8
8	0.06437	261.5
9	0.06836	273.4
10	0.08987	359.5

ANSYS finite element modeling (FEM) package. Mass and stiffness matrices M and K were obtained. Viscous and structural damping losses were added to the model by introducing a damping matrix C such that $C = b_0 I + c_0 K$, where $[b_0, c_0] = [0.0001, 0.0005]$. The first three mode shapes are shown in Fig. 5. The first 10 natural frequencies and damping ratios are listed in Table 4. The goal of this example is to develop an SMT that will exclusively excite and detect only the first two structural modes: The MPFs are thus selected such that $\alpha_{1,2} = 1/\lambda_1, 1/\lambda_2$, whereas all other MPFs are zero ($\lambda_j = \omega_j^2$, where ω_j^2 is the jth natural frequency).

Having determined the targeted subsystem mode shapes and selected MPFs, the piezoelectric field functions are then determined via Eq. (57). Based on the MPF values and data given in Tables 2 and 3, field function descriptions for each of the six active layers are found via numerically approximating each mode shape as a sixth-order polynomial in both α_1 and α_2 and then applying Eq. (57). The six required PFFs for layers 1–3 and 6–8 are shown in Fig. 6. The corresponding set of scaling factors g_0^k for layers 1–3 and 6–8 were found to be 3.17, 1.34, 1.45, 2.74, 1.44, and 1.64, respectively.

Having completed the design process, the SMT design would normally be implemented on the actual structure. For the purpose of verifying the SMT theory, actual structural implementation is replaced here with a numerical simulation. Premultiplying Eq. (43) by $\rho h A_1 A_2$ and recalling that $V^k(t) = g_0^k V_a(t)$ such that

$$\rho h A_1 A_2 \boldsymbol{x}_{tt} + \rho h A_1 A_2 \mathcal{C} \boldsymbol{x}_t + \rho h A_1 A_2 \mathcal{K} \boldsymbol{x} = -\left[\mathcal{D}^T \left(\sum_{k=1}^{N} g_0^k \boldsymbol{e}_0^k \Lambda^k \right) \right] V_a \tag{66}$$

the FEM model was derived by ignoring the RHS and discretizing the left-hand side of Eq. (66) so as to arrive at a numerical model in the form

$$M\ddot{\boldsymbol{x}} + C\dot{\boldsymbol{x}} + K\dot{\boldsymbol{x}} = 0 \tag{67}$$

where $\boldsymbol{x}$ is a time-dependent vector of $\alpha_1, \alpha_2, \alpha_3$ displacements at each node location. Using the piezofield functions just determined, the state equations are augmented through the discretization of the RHS of Eq. (66):

$$M\ddot{\boldsymbol{x}} + C\dot{\boldsymbol{x}} + K\boldsymbol{x} = \boldsymbol{f} V_a \tag{68}$$

Then, limiting the amount of modes of interest to 20 for the purpose of simulation, a modal transformation of the form $\boldsymbol{x} = V\boldsymbol{q}$ was performed on Eq. (68), where V is a matrix whose columns are the first 20-eigenvectors of Eq. (68) and $\boldsymbol{q}$ is a 20-element column vector containing the first 20 modal coordinates. The modal system representation is then given as

$$\ddot{\boldsymbol{q}} + \bar{C}\dot{\boldsymbol{q}} + \bar{K}\boldsymbol{q} = \boldsymbol{f}_q V_a(t) \tag{69}$$

where $\bar{C}$ and $\bar{K}$ are diagonal matrices whose respective elements contain the terms $b_0 + c_0\lambda_m$ and λ_m. Rewriting Eq. (69) in first-order

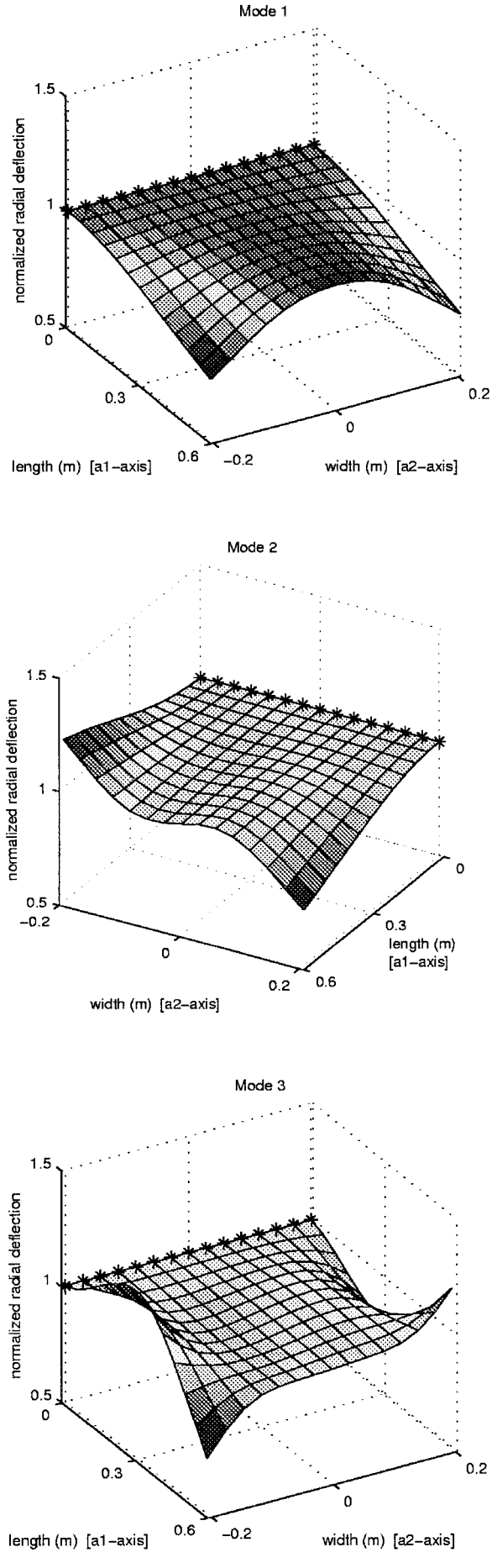

Fig. 5 First three structural mode shapes in curvilinear coordinate frame (deflections are scaled); starred boundary indicates a clamped condition.

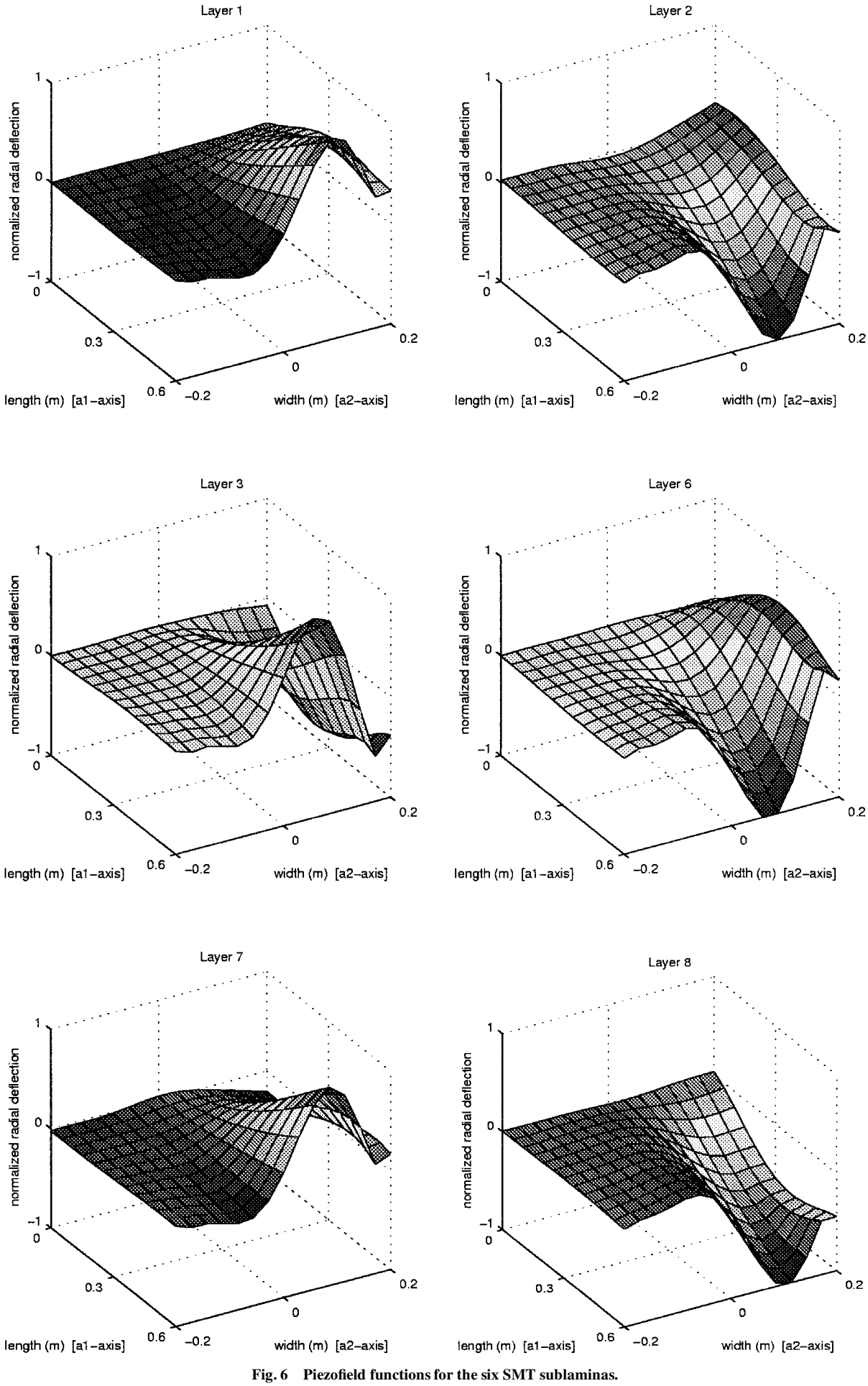

Fig. 6 Piezofield functions for the six SMT sublaminas.

form and including Eq. (44) in discretized form, the augmented system equations are

$$\frac{\mathrm{d}}{\mathrm{d}t}\begin{bmatrix}\boldsymbol{q}\\ \dot{\boldsymbol{q}}\end{bmatrix}=\begin{bmatrix}\mathbf{0} & \mathbf{1}\\ -\bar{K} & -\bar{C}\end{bmatrix}\begin{bmatrix}\boldsymbol{q}\\ \dot{\boldsymbol{q}}\end{bmatrix}+\begin{bmatrix}\mathbf{0}\\ \boldsymbol{f}_q\end{bmatrix}V_a \tag{70}$$

$$i=\begin{bmatrix}\mathbf{0} & \boldsymbol{f}_q^T\end{bmatrix}\begin{bmatrix}\boldsymbol{q}\\ \dot{\boldsymbol{q}}\end{bmatrix} \tag{71}$$

where $i(t)\triangleq(1/\rho h)i_s(t)$.

The SMT theory is itself validated by virtue of the observation that the elements of $\boldsymbol{f}_q$ are very nearly equal to $\alpha_m\lambda_m$, with marginal errors attributable to numerical differentiation. In particular,

$$\{\boldsymbol{f}_q(1:5)\}_{\text{actual}}=[1.136\quad 0.893\quad 0.000571\quad 0.0258\quad 0.0238]^T \tag{72}$$

Hence, error in the first mode was 13.6% and for the second mode 10.7%, whereas all MPFs corresponding to modes 3–20 were characterized by nonzero, albeit small, values. The Bode magnitude and phase plots of the transfer function $i(s)/V_a(s)$ are given in Fig. 7 and further illustrate the effectiveness of the design approach. Modes $m\geq 3$ are essentially not visible on the Bode plot because all MPFs for those modes have been set to zero. The peak amplitude of modes 1 and 2 should have been 0 dB had the numerical approximations been perfect, but instead deviate slightly. The most significant source of error was in fitting the mode shape estimates to polynomic functions (for differentiation), which essentially is a nonquantifiable error source but reasonably associated with observed error margins.

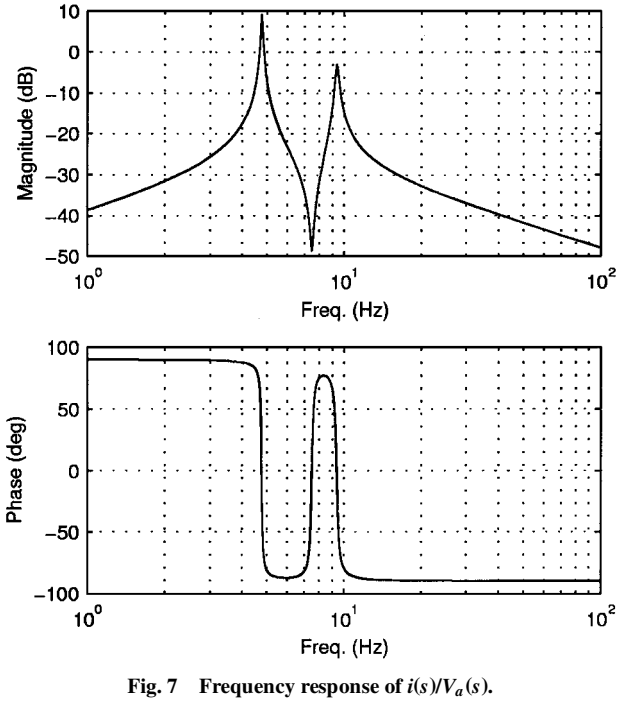

Fig. 7 Frequency response of $i(s)/V_a(s)$.

V. Conclusions

SMTs are developed for piezolaminated anisotropic shells in which the contribution of each mode to the sensing or excitation of the composite anisotropic plate system may be selectively weighted. The discussion has been limited to zero-Gaussian thin shell geometries well described by Love's first approximation theory. SMTs are formed by combining the piezoelectric effect of several piezolaminas. The SMT theory provides the basis for a design methodology in which the number and spatial field properties of piezoelectric sublaminas can be selected to yield transducers with a specified modal response. In a future paper, the theory is incorporated into a SMC strategy, wherein both control laws and piezofield functions are determined optimally for a broad class of performance metrics. The SMT theory can also be used in a converse sense to determine the modal character of a given piezolaminated shell structure. These SMT-based strategies provide a powerful tool for designing state-of-the-art active composite substructures as composite fabrication techniques further advance.

Appendix: Definitions

The differential operator $\mathcal{D}$ is defined as

$$\mathcal{D}\triangleq\begin{bmatrix}
-\dfrac{\partial}{\partial\alpha_1}\cdot A_2 & \left(\dfrac{\partial A_1}{\partial\alpha_2}\right) & \dfrac{A_1A_2}{R_1}\\
\left(\dfrac{\partial A_2}{\partial\alpha_1}\right) & -\dfrac{\partial}{\partial\alpha_2}\cdot A_1 & \dfrac{A_1A_2}{R_2}\\
-\left[\dfrac{\partial}{\partial\alpha_2}\cdot A_1+\left(\dfrac{\partial A_1}{\partial\alpha_2}\right)\right] & -\left[\dfrac{\partial}{\partial\alpha_1}\cdot A_2+\left(\dfrac{\partial A_2}{\partial\alpha_1}\right)\right] & 0\\
-\dfrac{1}{R_1}\dfrac{\partial}{\partial\alpha_1}\cdot A_2 & \dfrac{1}{R_2}\left(\dfrac{\partial A_1}{\partial\alpha_2}\right) & \mathcal{D}_{43}\\
\dfrac{1}{R_1}\left(\dfrac{\partial A_2}{\partial\alpha_1}\right) & -\dfrac{1}{R_1}\dfrac{\partial}{\partial\alpha_2}\cdot A_1 & \mathcal{D}_{53}\\
-\dfrac{1}{R_1}\left[\dfrac{\partial}{\partial\alpha_2}\cdot A_1+\left(\dfrac{\partial A_1}{\partial\alpha_2}\right)\right] & -\dfrac{1}{R_2}\left[\dfrac{\partial}{\partial\alpha_1}\cdot A_2+\left(\dfrac{\partial A_2}{\partial\alpha_1}\right)\right] & \mathcal{D}_{63}
\end{bmatrix} \tag{A1}$$

where the suboperators $\mathcal{D}_{43}$, $\mathcal{D}_{53}$, and $\mathcal{D}_{63}$ are given by

$$\mathcal{D}_{43}\triangleq\left[\frac{\partial}{\partial\alpha_2}\cdot\left(\frac{1}{A_2}\frac{\partial A_1}{\partial\alpha_2}\right)-\frac{\partial}{\partial\alpha_1}\cdot\frac{1}{A_1}\cdot\frac{\partial}{\partial\alpha_1}\cdot A_2\right] \tag{A2}$$

$$\mathcal{D}_{53}\triangleq\left[\frac{\partial}{\partial\alpha_1}\cdot\left(\frac{1}{A_1}\frac{\partial A_2}{\partial\alpha_1}\right)-\frac{\partial}{\partial\alpha_2}\cdot\frac{1}{A_2}\cdot\frac{\partial}{\partial\alpha_2}\cdot A_2\right] \tag{A3}$$

and

$$\mathcal{D}_{63}\triangleq-\left\{\frac{\partial}{\partial\alpha_1}\cdot\frac{1}{A_1}\cdot\left[\frac{\partial}{\partial\alpha_1}\cdot A_1+\left(\frac{\partial A_1}{\partial\alpha_2}\right)\right]+\frac{\partial}{\partial\alpha_2}\cdot\frac{1}{A_2}\cdot\left[\frac{\partial}{\partial\alpha_1}\cdot A_2+\left(\frac{\partial A_2}{\partial\alpha_1}\right)\right]\right\} \tag{A4}$$

The operator $\mathcal{E}$ is defined as

$$\mathcal{E} \triangleq \begin{bmatrix} A_2\frac{\partial}{\partial\alpha_1} & \left(\frac{\partial A_1}{\partial\alpha_2}\right) & \frac{A_1A_2}{R_1} \\ \left(\frac{\partial A_2}{\partial\alpha_1}\right) & A_1\frac{\partial}{\partial\alpha_2} & \frac{A_1A_2}{R_2} \\ A_1^2\frac{\partial}{\partial\alpha_2}\cdot\frac{1}{A_1} & A_2^2\frac{\partial}{\partial\alpha_1}\cdot\frac{1}{A_2} & 0 \\ A_2\frac{\partial}{\partial\alpha_1}\cdot\frac{1}{R_1} & \left(\frac{\partial A_1}{\partial\alpha_2}\right)\frac{1}{R_2} & -\left[A_2\frac{\partial}{\partial\alpha_1}\cdot\frac{1}{A_1}\cdot\frac{\partial}{\partial\alpha_1}+\frac{1}{A_2}\left(\frac{\partial A_1}{\partial\alpha_2}\right)\frac{\partial}{\partial\alpha_2}\right] \\ \left(\frac{\partial A_2}{\partial\alpha_1}\right)\frac{1}{R_1} & A_1\frac{\partial}{\partial\alpha_2}\cdot\frac{1}{R_2} & -\left[A_1\frac{\partial}{\partial\alpha_2}\cdot\frac{1}{A_2}\cdot\frac{\partial}{\partial\alpha_2}+\frac{1}{A_1}\left(\frac{\partial A_2}{\partial\alpha_1}\right)\frac{\partial}{\partial\alpha_1}\right] \\ A_1^2\frac{\partial}{\partial\alpha_2}\cdot\frac{1}{A_1R_1} & A_2^2\frac{\partial}{\partial\alpha_1}\cdot\frac{1}{A_2R_2} & -\left[A_2^2\frac{\partial}{\partial\alpha_1}\cdot\frac{1}{A_2^2}\cdot\frac{\partial}{\partial\alpha_2}+A_1^2\frac{\partial}{\partial\alpha_2}\frac{1}{A_1^2}\frac{\partial}{\partial\alpha_1}\right] \end{bmatrix} \tag{A5}$$

The transverse shear force resultants are defined as[13]

$$Q_4 \triangleq -\frac{1}{A_1A_2}\left[\mathcal{D}_{11}M_1 + M_2\frac{\partial A_2}{\partial\alpha_1} + \mathcal{D}_{31}M_6\right]$$

$$Q_5 \triangleq -\frac{1}{A_1A_2}\left[M_1\frac{\partial A_1}{\partial\alpha_2} + \mathcal{D}_{22}M_2 + \mathcal{D}_{32}M_6\right] \tag{A6}$$

The orthotropic stiffness suboperators are defined as

$$\mathcal{D}_s \triangleq \begin{bmatrix} -\frac{\partial}{\partial\alpha_1}\cdot A_1 & \left(\frac{\partial A_1}{\partial\alpha_2}\right) \\ \left(\frac{\partial A_2}{\partial\alpha_1}\right) & -\frac{\partial}{\partial\alpha_2}\cdot A_1 \\ -\left[\frac{\partial}{\partial\alpha_2}\cdot A_1 + \left(\frac{\partial A_1}{\partial\alpha_2}\right)\right] & -\left[\frac{\partial}{\partial\alpha_1}\cdot A_2 + \left(\frac{\partial A_2}{\partial\alpha_1}\right)\right] \end{bmatrix} \tag{A7}$$

$$\mathcal{E}_s \triangleq \begin{bmatrix} A_2\frac{\partial}{\partial\alpha_1} & \left(\frac{\partial A_1}{\partial\alpha_2}\right) \\ \left(\frac{\partial A_2}{\partial\alpha_1}\right) & A_1\frac{\partial}{\partial\alpha_2} \\ A_1^2\frac{\partial}{\partial\alpha_2}\cdot\frac{1}{A_1} & A_2^2\frac{\partial}{\partial\alpha_2}\cdot\frac{1}{A_2} \end{bmatrix} \tag{A8}$$

$$\mathcal{D}_b \triangleq \begin{bmatrix} \left[\frac{\partial}{\partial\alpha_2}\cdot\left(\frac{1}{A_2}\frac{\partial A_1}{\partial\alpha_2}\right) - \frac{\partial}{\partial\alpha_1}\cdot\frac{1}{A_1}\cdot\frac{\partial}{\partial\alpha_1}\cdot A_2\right] \\ \left[\frac{\partial}{\partial\alpha_1}\cdot\left(\frac{1}{A_1}\frac{\partial A_2}{\partial\alpha_2}\right) - \frac{\partial}{\partial\alpha_2}\cdot\frac{1}{A_2}\cdot\frac{\partial}{\partial\alpha_2}\cdot A_1\right] \\ -\left\{\frac{\partial}{\partial\alpha_1}\cdot\frac{1}{A_1}\cdot\left[\frac{\partial}{\partial\alpha_2}\cdot A_1 + \left(\frac{\partial A_1}{\partial\alpha_2}\right)\right] + \frac{\partial}{\partial\alpha_2}\cdot\frac{1}{A_2}\cdot\left[\frac{\partial}{\partial\alpha_1}\cdot A_2 + \left(\frac{\partial A_2}{\partial\alpha_1}\right)\right]\right\} \end{bmatrix} \tag{A9}$$

$$\epsilon_2 \triangleq \begin{bmatrix} -\left[A_2\frac{\partial}{\partial\alpha_1}\cdot\frac{1}{A_1}\cdot\frac{\partial}{\partial\alpha_1}+\frac{1}{A_2}\left(\frac{\partial A_1}{\partial\alpha_2}\right)\frac{\partial}{\partial\alpha_2}\right] \\ -\left[A_1\frac{\partial}{\partial\alpha_2}\cdot\frac{1}{A_2}\cdot\frac{\partial}{\partial\alpha_2}+\frac{1}{A_1}\left(\frac{\partial A_2}{\partial\alpha_1}\right)\frac{\partial}{\partial\alpha_1}\right] \\ -\left[A_2^2\frac{\partial}{\partial\alpha_1}\cdot\frac{1}{A_2^2}\cdot\frac{\partial}{\partial\alpha_2}+A_1^2\frac{\partial}{\partial\alpha_2}\frac{1}{A_1^2}\frac{\partial}{\partial\alpha_1}\right] \end{bmatrix} \tag{A10}$$

References

[1]Bailey, T., and Hubbard, J., "Distributed Piezoelectric Polymer Active Vibration Control of a Cantilever Beam," *Journal of Guidance, Control, and Dynamics*, Vol. 8, No. 5, 1985, pp. 605–611.

[2]Hubbard, J. E., "Method and Apparatus Using a Piezoelectric Film for Active Vibration Control of Vibrations," U.S. Patent No. 4565940, 1986.

[3]Burke, S., and Hubbard, J. E., "Distributed Actuator Control Design for Flexible Beams," *Automatica*, Vol. 24, No. 5, 1988, pp. 619–627.

[4]Miller, S. E., and Hubbard, J. E., "Observability of a Bernouli–Euler Beam Using PVF2 as a Distributed Sensor," *Dynamics and Control of Large Structures*, edited by L. Meirovitch, Virginia Polytechnic Inst. and State Univ., Blacksburg, VA, 1987, pp. 375–390.

[5]Miller, S. E., and Hubbard, J. E., "Smart Components for Structural Vibration Control," *Proceedings of the 1988 American Controls Conference*, Vol. 3, Inst. of Electrical and Electronics Engineers, New York, 1988, pp. 1897–1902.

[6]Burke, S. E., and Hubbard, J. E., "Distributed Transducer Control Design for Thin Plates," *Proceedings of the Conference on Electro-Optical Materials for Switches, Coatings, Sensor Optics, and Detectors*, Vol. 1307, Society of Photo-Optical Instrumentation Engineers, Bellingham, WA, 1990, pp. 222–231.

[7]Ashton, J. E., Halpin, J. C., and Petit, P. H., *Primer on Composite Materials: Analysis*, Vol. 3, Progress in Material Science Series, Technomic Press, Stamford, CT, 1969, pp. 14–16.

[8]Lee, C. K., "Theory of Laminated Piezoelectric Plates for the Design of Distributed Sensors and Actuators. Part 1: Governing Equations and Reciprocal Relationships," *Journal of the Acoustical Society of America*, Vol. 87, No. 3, 1990, pp. 1144–1158.

[9]Miller, S., Abramovich, H., and Oshman, Y., "Active Distributed Vibration Control of Anisotropic Piezoelectric Laminated Plates," *Journal of Sound and Vibration*, Vol. 183, No. 5, 1995, pp. 797–817.

[10]Miller, S. E., Oshman, Y., and Abramovich, H., "Modal Control of Piezolaminated Anisotropic Rectangular Plates. Part 2: Control Theory," *AIAA Journal*, Vol. 34, No. 9, 1996, pp. 1876–1884.

[11]Miller, S. E., Oshman, Y., and Abramovich, H., "Modal Control of Piezolaminated Anisotropic Rectangular Plates. Part 1: Transducer Theory," *AIAA Journal*, Vol. 34, No. 9, 1996, pp. 1868–1875.

[12]Reddy, J. N., *Energy and Variational Methods in Applied Mechanics*, Wiley, New York, 1984, pp. 183–195.

[13]Soedel, W., *Vibrations of Shells and Plates*, Dekker, New York, 1981,

pp. 229–235.
[14]Bert, C. W., Baker, J. L., and Egle, D. M., "Free Vibrations of Multilayer Anisotropic Cylindrical Shells," *Journal of Composite Materials*, Vol. 3, July 1969, pp. 480–499.
[15]Love, A. E. H., *A Treatise on Mathematical Theory of Elasticity*, 4th ed., Dover, New York, 1944, pp. 43–56.
[16]*Piezolectricity*, ANSI/IEEE Standard 176, Inst. of Electrical and Electronics Engineers, New York, 1987.
[17]Miller, S. E., and Abramovich, H., "A Self-Sensing Piezolaminated Actuator Model for Shells Using a First Order Shear Deformation Theory," *Journal of Intelligent Material Systems and Structures*, Vol. 6, No. 5, 1995, pp. 624–638.
[18]Dias, C., Wenger, M., Blanas, P., Shuford, J., Hinton, Y., and Das-Gupta, D. K., "Intelligent Piezoelectric Composite Materials for Sensors," *Proceedings of the 2nd International Conference on Intelligent Materials* (Williamsburg, VA), edited by C. A. Rogers and G. G. Wallace, Technomic, Lancaster, PA, 1994, pp. 437–449.
[19]Meirovitch, L., *Dynamics and Control of Structures*, Wiley, New York, 1990, pp. 180–182.
[20]Dosch, J., Mayne, R., and Inman, D., *Dual Function System Having A Piezoelectric Element*, U.S. Patent No. 5347870, 1994.
[21]Inman, D. J., "Modal Decoupling Conditions for Distributed Control of Flexible Structures," *Journal of Guidance, Control, and Dynamics*, Vol. 7, No. 6, 1984, pp. 750–752.
[22]Caughey, T. K., and O'Kelly, M. E. J., "Classical Normal Modes in Damped Linear Dynamic Systems," *Journal of Applied Mechanics*, Vol. 32, Sept. 1965, pp. 583–588.
[23]Miller, S. E., "Distributed Modal Control of Piezolaminated Anisotropic Planar and Cylindrical Structures," Doctor of Science Dissertation, Faculty of Aerospace Engineering, Technion—Israel Inst. of Technology, Haifa, Israel, Sept. 1995.
[24]Miller, S. E., Abramovich, H., and Oshman, Y., "Experimental Validation of a Modal Transducer for an Orthotropic Rectangular Plate," *AIAA Journal*, Vol. 35, No. 10, 1997, pp. 1621–1629.